

3D TEXTURE SYNTHESIS FOR MODELING REALISTIC ORGANIC TISSUES

Juan-Carlos Prieto¹, Chantal Revol-Muller¹, Françoise Peyrin^{1,2}, Patrizia Camelliti³
and Christophe Odet¹

¹CREATIS, CNRS UMR 5220, Inserm U1044, Univ. de Lyon1, INSA-Lyon, 7 Avenue Jean Capelle 69621, Lyon, France

²ESRF, BP 220, 38043 Grenoble, France

³NHLI, Imperial College London, London, U.K.

Keywords: 3D Texture Synthesis, Image-based Modeling, Organ Modeling, Histology, Patient-specific, Image/Mechanical Simulation, Virtual Human.

Abstract: Virtual anatomy models show in detail characteristics of the human body systems. These models are based in surface representation of the structures and lack information from the interior of the object. Creating models that represent the surface, the interior of the object and are able to provide pathological information is the current challenge of research in life sciences. We present a method to synthesize realistic three-dimensional organic tissues starting from bidimensional textured multi-channel samples. The method relies on an energy function that measures the difference between the reference texture and the synthesized object, through a distance metric that compares perpendicular neighborhoods in the object to neighborhoods in the sample. When this function is minimized by IRLS, the result is a solid object that resembles the sample at every slice. In some cases, the optimization might be aided by adding the feature distance transform, calculated from a given binary mask. This allows to code large textured areas. Multiple textures can also be provided to the optimization in order to create anisotropic textures. We apply our method starting from various micrometric images such as histology images or slices of Synchrotron Radiation Computed Micro-Tomography (SR μ CT) images. A major advantage of our method is to extend 2D histological information to a 3D representation. We demonstrate the accuracy of the generated texture by comparing statistical and morphological parameters computed from the synthetic object with those obtained from the real object underlying the reference images.

1 INTRODUCTION

Realistic modeling of the human body is the current challenge in research of life sciences, projects around the world such as VPH-NOE (Virtual Physiological Human - Network of Excellence)¹ aim to create computer models for personalized and predictive healthcare. The main goal is to create models capable of integrating not only anatomical information but also physiological, mechanical and the biochemical processes related to the organ.

There are human anatomy models such as the Google Body Browser² or the Visible Body³, they offer a detailed 3D view of the human body systems (digestive, nervous, skeletal etc.), and are based in su-

rface representations of the structures. These models are organized in a multi-scale fashion, giving the possibility to navigate through the body system, they are mainly used as a learning tool, as they are not conceived to be used for patient-specific analysis or planning purposes. These models have another limitation such as the lack of information at different scales *e.g.* the structure of the bone tissue is not available.

Modeling different types of organs and tissues at the cellular level represents an interest for histology *i.e.* the study of tissues. Histology plays an important role in the comprehension of morphological relationships between the organs and tissues, as it considers the structural organization or precise hierarchy of the organs with the smallest details. This represents an advantage as tissues are formed by cells, we could have structural information at different scales.

In this paper, we propose a method generic enough that is able to reproduce complex 3D objects, by us-

¹<http://www.vph-noe.eu/>

²<http://bodybrowser.googlelabs.com/body.html>

³<http://www.visiblebody.com/>

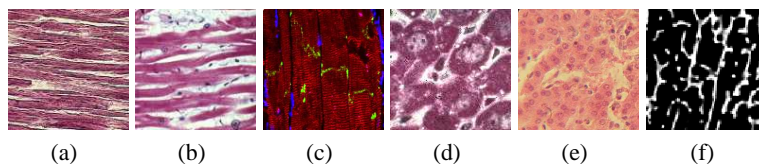


Figure 1: 128^2 textured samples available to create volumetric data: (a) skeletal muscle sample artistically created; histology images of (b) striated cardiac muscle, (c) myocytes, (d-e) hepatocytes; (f) a slice from a SR μ CT image of a trabecular bone sample.

ing 2D textured samples. Our method derives from Kopf's approach (Kopf et al., 2007), it starts with a 2D reference image and by means of an energy optimization process described by Kwatra (Kwatra et al., 2005), it is able to create a 3D texture that resembles the 2D image in every slice. The reference 2D images can illustrate any textured element and can be of different kinds: i) artificial images artistically created for computer graphic design or medical atlases or ii) real images with very complex texture provided by digital microscopy of biomedical histological slices. Figure 1 show samples of textured images, available to produce different types of volumetric data.

The texture synthesis optimization has the advantage to be able to constraint separately the axial, longitudinal and transversal planes of the 3D texture by taking into account one or multiple reference textures. Moreover, extra channels can be added to the exemplar, like distance maps when large texture features must be coded (Lefebvre and Hoppe, 2006).

The method also maintains the global statistics of the sample by using a histogram matching approach presented by (Rolland et al., 2000) and (Heeger and Bergen, 1995).

In the remainder of this paper, we present in detail our method to synthesize realistic 3D textures modeling organic tissues and provide an overview of the different types of texture that can be generated. As we shall show in the section 4, the accuracy of the 3D synthetic texture is demonstrated by comparing statistical and morphological parameters computed from both the synthetic texture and the reference object.

2 METHOD

2.1 3D Texture Synthesis

3D texture synthesis has been used before to create realistic solid objects, giving the possibility to perform scattering simulations or cut through them. Our approach is based on an energy proposed by (Kwatra et al., 2005) and defined by the following equation:

$$E(o, \{e\}) = \sum_t \sum_{i \in \{x,y,z\}} \|o_{t,i} - e_{t,i}\|^r \quad (1)$$

It is based on a distance metric that compares the neighborhoods x , y , z of a texel t in the object o and neighborhoods from the sample texture e . When minimized, using IRLS (iterative re-weighted least squares), the result is an increase of similarity between the sample and the synthetic object.

The procedure begins at a coarse resolution assigning random values from the sample to the synthetic object. Then, it alternates between a search phase where the closest neighborhoods are found and an optimization phase where the weighted average of every texel is calculated. When the optimization converges, it changes to a finer resolution level using linear interpolation.

2.1.1 Search Phase

The sample image is divided into 9×9 neighborhoods that overlap each other, these neighborhoods are vectorized *i.e.* every texel from the neighborhood is stacked into a single vector. For RGB texels we have $9 \times 9 \times 3 = 243$ values in a single vector. It is possible to use a distance map as an extra channel by giving the algorithm a binary image as input, this is useful when the texture has large unstructured areas. Once the vectors from the sample are constructed, we apply PCA (principal component analysis)⁴ to reduce the dimensionality of each vector passing from 243 to 18 values approximately.

Reducing the vectors is a very convenient step, there are less values but we are still keeping 95% of the relevant information. The reduced vectors can be used to perform a standard closest neighborhood search in a high dimensional space. For this purpose, we use ANN library⁵.

⁴L. Smith 2002, A Tutorial on Principal Components Analysis; www.cs.otago.ac.nz/cosc453/student_tutorials/principal_components.pdf

⁵ANN: A library for approximate nearest neighbor searching; <http://www.cs.umd.edu/~mount/ANN/> Mount, D. M. and Arya, S. 2006.

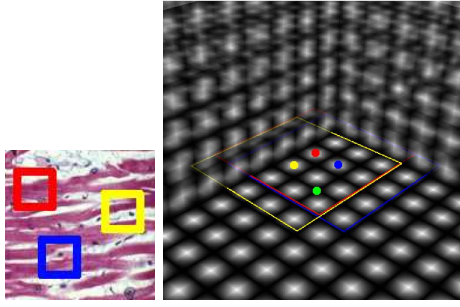


Figure 2: 9x9 red, blue and yellow neighborhoods for a slice in the volume, the center is represented by the colored dot. The green voxel is affected by multiple neighborhoods.

$$E(o, \{e\}) = \sum_t \sum_{i \in \{x,y,z\}} \sum_{u \in N_i(t)} w_{t,i,u} (o_{t,i,u} - e_{t,i,u})^2 \quad (2)$$

$$w_{t,i} = \|o_{t,i} - e_{t,i}\|^{r-2} \quad (3)$$

During the search phase a weight for each neighborhood is calculated, for this purpose the energy function is written as equation 2 and the weight is calculated as shown in equation 3. $N_i(t)$ represents the neighborhoods found in each dimension x, y, z and u is the texel in the neighborhood of t , this means that a texel in the object is affected by multiple texels from different neighborhoods in the exemplar texture. The search is performed for every two texels $g_x = \{(i, 2 * j, 2 * k), \forall i, j, k\}$, g_x is the voxel in a slice perpendicular to x . This is done similarly for y and z , as shown in figure 2. We set $r = 0.8$ to perform a robust optimization (Kwatra et al., 2005).

Once the search phase is done the optimization phase takes place and it consists in averaging all the values found for each texel of the volume.

2.1.2 Optimization Phase

The optimization phase consists in averaging the values that affect one texel in the object. Note that if the search phase is performed for every two texels as in 2.1.1, then the average will be for at most 75 texels (25 for each dimension).

$$o_t = \frac{\sum_{i \in \{x,y,z\}} \sum_{u \in N_i(t)} w_{u,i,t} * e_{u,i,t}}{\sum_{i \in \{x,y,z\}} \sum_{u \in N_i(t)} w_{u,i,t}} \quad (4)$$

Equation 4 shows the value of a texel in the object. When the texels present a high variability, the resulting object might be blurred, in order to avoid this, clustering is performed to only average those texels that correspond to the principal cluster.

Following the optimization phase, the histogram matching is done to preserve the global statistics of the object relative to the exemplar.

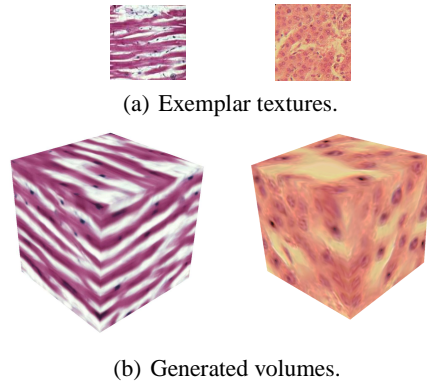


Figure 3: Results of isotropic synthesis. The striated cardiac muscle tissue (left) and liver cell tissue (right) were generated using a single reference texture for the axial, longitudinal and transversal planes.

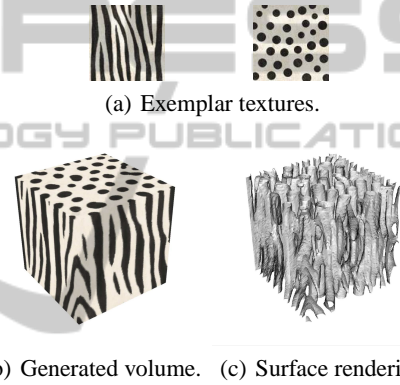


Figure 4: Results of anisotropic synthesis. The optimization was performed using the zebra texture to constraint the longitudinal and transversal planes. The dot texture was used in the axial plane.

2.1.3 Histogram Matching

To perform histogram matching, the *CDF* (cumulative distribution function) is calculated for both the exemplar and the object. Two *LUTs* are constructed in order to perform faster calculations. The lookup table LUT_o maps the RGB values of the object to their corresponding value in the CDF_o , the lookup table LUT_e maps the CDF_e to the corresponding RGB values from the sample. The object is then modified by taking each of the texels t , using $LUT_o(t)$ to find the $CDF_o(t)$ and then using $LUT_e(CDF_o(t))$ to find the corresponding RGB value from the sample. The value of the object is then replaced by the corresponding value of the sample.

3 RESULTS

The algorithm was implemented in C++ using ITK⁶ for image processing and VTK⁷ for visualization. Using ITK allowed the image processing to be performed in parallel, thus gaining computational time. Synthetic 3D images of both 128^3 pixels and 256^3 pixels were generated using different type of textures, from histology images acquired with a digital microscope.

3.1 Isotropic Texture from a 2D Exemplar Texture

Figure 3 shows some results when the same exemplar is used to perform the optimization in the perpendicular planes of each three axis. Our method allows the 3D synthesis of the striated cardiac muscle tissue and the liver cell tissue from only one histology slice. It can be noted that any axial, longitudinal or transversal slice of the volume is similar to the reference texture without being, however, identical.

3.2 Anisotropic Texture from Many 2D Exemplar Textures

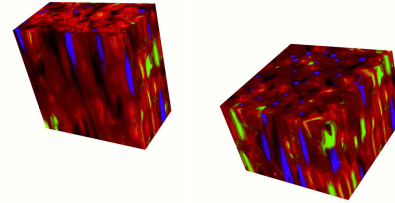
Figure 4 shows the result of selecting two different textures to constraint the optimization. Selecting the zebra texture for the longitudinal and transversal planes with the dot pattern for the axial plane generated cylinder like structures. When rendering the surface of the object, we can see that the generated structure is very complex and consists of tubes that join and separate at arbitrary slices. This synthetic structure was used in our lab to test Brownian simulation algorithms that reveal the environment's structures.

3.3 Anisotropic Texture Constrained by Additional Masks

Figure 5 shows the synthesis results using different exemplar textures obtained from confocal images⁸ and extra channels provided by signed Euclidean distance maps computed from binary masks. The 3D texture representing a myocyte cell tissue are quite representative of cells organisation (myocytes in red and fibroblasts in blue). The anisotropy of the cells is conspicuous and the contrast of staining is well preserved thanks to the use of the binary masks.



(a) Exemplar textures + binary masks.



(b) Longitudinal view of the volume. (c) Axial view of the volume.

Figure 5: Results of anisotropic synthesis starting from two different textures and their additional binary masks.

One main advantage of our method is to generate a 3D tissue from 2D information. Up to now, it was impossible for the biologist or the physician to have a 3D representation of the cell tissue, since it is technically very difficult or even impossible to have an axial resolution as good as those in the slice. Thanks to our approach, the experts can get a virtual 3D representation of the tissues that are close to reality without being it.

4 EVALUATION AND DISCUSSION

We propose to assess the quality of our synthetic 3D texture according to two criteria: statistical and morphological accuracy. As the ultimate goal of our work is to produce a 3D texture as close as possible to the reference object, we will compare statistical and morphological features computed from the reference object with to those computed from the synthetic texture.

4.1 Statistical Assessment

Figure 6 shows the histograms from the exemplar texture and the synthesized object shown in figure 3. The total number of pixels in the texture are $128^2 = 16384$ and $128^3 = 2097152$ for the volume. Note that when a randomly chosen slice is taken from the volume, the global statistics are still preserved. Table 1 contains the means and the standard deviations calculated from the histograms, the values from the object are similar to those of the exemplar with a variation lower than 1% for the means and lower than 2% for the standard deviations.

⁶<http://www.itk.org>

⁷<http://www.vtk.org>

⁸<http://www1.ic.ac.uk/medicine/people/p.camelliti/>

Table 1: Means and standard deviations for the RGB channels of the exemplar and the object.

		Mean	St. Dev
Red	<i>e</i>	189.6	34.7
	<i>o</i>	188.7	34.0
Green	<i>e</i>	142.4	70.2
	<i>o</i>	141.4	69.3
Blue	<i>e</i>	168.8	48.7
	<i>o</i>	168.0	48.1

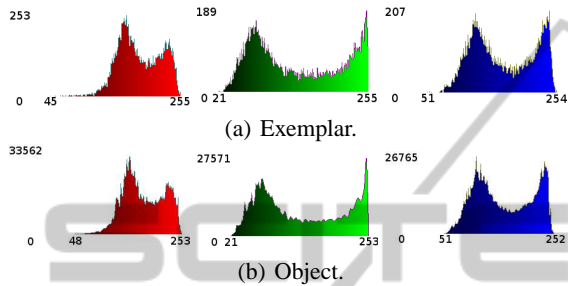


Figure 6: RGB histograms of the exemplar and the object for the striated cardiac muscle shown in figure 3.

4.2 Morphological Assessment

We propose to quantitatively assess the accuracy of the morphological structure given by our synthetic 3D texture. For this study, we generate a 3D texture from images provided by Synchrotron Radiation Computed Micro-Tomography (SR μ CT). These images were acquired few years ago on beam-line ID19 at the European Synchrotron Radiation Facility (ESRF) in Grenoble for the needs of a study focused on osteoporosis. Osteoporosis is a bone fragility disease leading to spontaneous bone fractures and characterized by a bone mass reduction and a bone structure deterioration. 3D Synchrotron Radiation Computed Micro-Tomography (SR μ CT) provided 3D high resolution images with an isotropic voxel of 10 μ m width and a volume size of 330 * 330 * 330 pixels helpful to assess trabecular bone architecture (Revol-Muller et al., 2002). Therefore, we have at our disposal a set of twelve 3D SR μ CT images obtained from twelve calcaneus bone samples excavated from deceased human. For the test of our method, we worked on decimated SR μ CT images with a resolution of 80 μ m and a size of 83 * 83 * 83 voxels. At this resolution, the signal to noise ratio is still high enough to extract trabecular bone from the background by simple automated thresholding. This binarizing step is needed for the computation of the bone parameters.

We computed morphologic and topological architecture parameters similar to those used in histomorphometry but computed on three-dimensional images

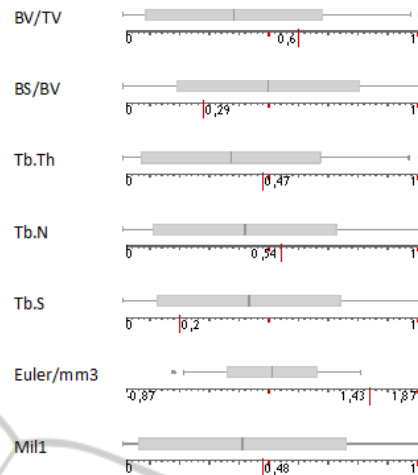


Figure 7: Box plots for morphologic and topological architecture of bones.

from the set of the twelve volumes. A 3D MIL (Mean Intercept Length) method based on a three-dimensional version of the directed secant algorithm was chosen to produce many parameters related to the trabecular bone morphology (Hipp and Simmons, 1997) and the Euler number was computed to estimate the bone topology. We considered the seven following parameters: Partial Bone Volume (BV/TV), Bone Surface to Bone Volume ratio (BS/BV), Trabecular Thickness (Tb. Th), Trabecular Number (Tb. N), Trabecular Separation (Tb. Sp) and Mean Intercept Length (MIL1). The connectivity was estimated by the Euler number (Euler/mm³) implemented following the method described in (Odgaard and Gundersen, 1993) and normalized by the total volume. The higher the Euler number's value, the less connected the bone structure is.

We generated by our method a 3D SR μ CT-like texture (128 * 128 * 128 voxels) from two random reference slices (83 * 83 pixels) taken into one out of the twelve SR μ CT volumes. We binarized the texture in order to extract the virtual bone architecture by the same automated thresholding than that used for the set of SR μ CT volumes. Then we assess the accuracy of the virtual bone structure by comparing the bone parameters computed from the set of SR μ CT images with those computed from the synthetic 3D volume.

Figure 7 displays the box plots associated to each bone parameter obtained from the set of SR μ CT images. As our aim is not focused on the analysis or the interpretation of these parameters but only on the comparison of them, we normalized each parameter by the range between their maximum and minimum values. The score of the synthetic texture is displayed on the scale line under each box plot by a long red

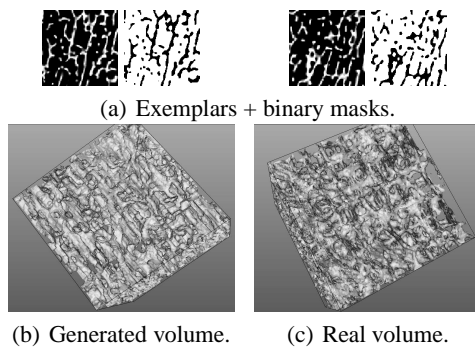


Figure 8: Anisotropic synthesis with additional binary masks. Surface rendering of trabecular bone architecture obtained with the synthetic texture and the SR μ CT image.

line. It can be noticed that for all the morphologic parameters the score for the virtual bone is spread in a range lower than \pm one standard deviation from the mean value obtained from the SR μ CT set, thus proving its resemblance with the architecture of real bone. For the topology parameter (Euler/mm³), the score is slightly higher than the maximum value obtained with the SR μ CT set, but that remains satisfying. It means that the virtual bone structure has a somewhat lower connectivity than the reference set. It could represent a high degree of osteoporosis.

In Figure 8, the surface of the virtual bone is compared to the surface of the 3D SR μ CT image from which were taken the reference slices for the texture synthesis. We retrieve visually the similarity demonstrated by the bone parameters.

5 CONCLUSIONS

Our method allows to create realistic organic tissue from small samples acquired by a digital microscope or other image acquisition devices such as Synchrotron Radiation Computed Micro-Tomography. We demonstrated quantitatively the accuracy of the synthetic texture from both statistical and morphological points of view. Latter tests showed that our synthetic objects like the zebra-dot 3D texture can be useful for simulation especially in the framework of Brownian simulation. In future work, we will use our method to enhance surface models. We will aim at coupling texture synthesis with minimal skeleton representations such as the m-reps developed by Pizer *et al.* (Pizer *et al.*, 2003) and reproducing the interior of the organs at multi-scale levels using 2D samples of tissue.

REFERENCES

- Heeger, D. J. and Bergen, J. R. (1995). Pyramid-based texture analysis/synthesis. In *Proceedings of the 22nd annual conference on Computer graphics and interactive techniques*, SIGGRAPH '95, pages 229–238, New York, NY, USA. ACM.
- Hipp, J. and Simmons, C. (1997). Method-based differences in the automated analysis of the three-dimensional morphology of trabecular bone. *Journal of Bone and Mineral Research*, 12.
- Kopf, J., Fu, C.-W., Cohen-Or, D., Deussen, O., Lischinski, D., and Wong, T.-T. (2007). Solid texture synthesis from 2d exemplars. *ACM Transactions on Graphics (Proceedings of SIGGRAPH 2007)*, 26(3):2:1–2:9.
- Kwatra, V., Essa, I., Bobick, A., and Kwatra, N. (2005). Texture optimization for example-based synthesis. *ACM Transactions on Graphics, SIGGRAPH 2005*.
- Lefebvre, S. and Hoppe, H. (2006). Appearance-space texture synthesis. *ACM Trans. Graph.*, 25:541–548.
- Odgaard, A. and Gundersen, H. (1993). Quantification of connectivity in cancellous bone, with special emphasis on 3d reconstructions. *Bone*, 14:173–182.
- Pizer, S. M., Fletcher, P. T., Joshi, S., Thall, A., Chen, J. Z., Fridman, Y., Fritsch, D. S., Gash, A. G., Glotzer, J. M., Jiroutek, M. R., Lu, C., Muller, K. E., Tracton, G., Yushkevich, P., and Chaney, E. L. (2003). Deformable m-reps for 3d medical image segmentation. *Int. J. Comput. Vision*, 55:85–106.
- Revol-Muller, C., Benoit-Cattin, H., Carillon, Y., Odet, C., Briguët, A., and Peyrin, F. (2002). Bone mri segmentation assessment based on synchrotron radiation computed microtomography. *IEEE Trans Nucl Sci*, 49(1):220–224.
- Rolland, J. P., Vo, V., Bloss, B., and Abbey, C. K. (2000). Fast algorithms for histogram matching: application to texture synthesis. *Journal of Electronic Imaging*, 9:39–45.